

# We are IntechOpen, the world's leading publisher of Open Access books Built by scientists, for scientists

4,800

Open access books available

122,000

International authors and editors

135M

Downloads

Our authors are among the

154

Countries delivered to

TOP 1%

most cited scientists

12.2%

Contributors from top 500 universities



WEB OF SCIENCE™

Selection of our books indexed in the Book Citation Index  
in Web of Science™ Core Collection (BKCI)

Interested in publishing with us?  
Contact [book.department@intechopen.com](mailto:book.department@intechopen.com)

Numbers displayed above are based on latest data collected.  
For more information visit [www.intechopen.com](http://www.intechopen.com)



## Chapter

# Corrosion Fatigue of Aluminum-Copper-Lithium Alloy 2050-T84 Submitted at Salt Spray and Aqueous Saline Solution

*Maciel Carla Isabel dos Santos,  
Bose Filho Waldek Wladimir and  
Ruchert Cassius Olívio Figueiredo Terra*

## Abstract

Interest in the improvement of the structural performance of aircraft has begun in the substitution of aluminum alloys due to the possibility of reduction of density, an increase of stiffness, high fracture toughness, greater resistance to the propagation of cracks by fatigue and greater resistance to corrosion. In these issues, the aluminum-copper-lithium alloy 2050-T84 is outstanding, which presents excellent mechanical properties even when subjected to aggressive atmospheres. The failure of structural components of aircraft occurs due to several factors that may arise from microstructural defects and/or applied static or cyclic stresses associated with atypical environments such as cryogenic or corrosive. In this sense, the results have evidenced the presence of precipitates that influence in the increase of the mechanical strength, behavior of fracture toughness, fatigue life, and corrosion fatigue, in different temperatures and aggressive means. Tensile and fracture toughness tests at 23 and  $-60^{\circ}\text{C}$  the material showed ductility retention without a significant difference in the results. Fatigue crack growth in air and corrosion fatigue with 3.5 and 5% NaCl and aqueous solution with 3.5% NaCl showed a meaning difference in the threshold region; however, for the Paris region at the saline environment, fatigue crack growth (FCG) rates are similar.

**Keywords:** corrosion fatigue,  $da/dN$ , Al-Cu-Li alloy, 2050-T84, mechanical behavior, salt spray, aqueous saline solution

## 1. Introduction

High strength heat hardening aluminum alloys are relevant for aeronautical applications due to their excellent interaction between chemical, physical and mechanical properties, and weight reduction. Such integration results in structures with maximum efficiency and fuel economy for aircraft in operation, based on this a large number of alloys has been developed in response. The aircraft industry is the symbols of technological generation and has developed improvements in structural

integrity with the replacement of aluminum alloys, safer aircraft, and reduction of the costs of manufacturing, maintenance and operation. Therefore, this technological sector develops research for optimization of projects that result in lighter aircraft with the direct consequence in the fuel consumption and operationally more viable.

Highlighting of the substitution of structural and fuselage materials, the proposal for the manufacture of aluminum-lithium alloys showed up attractive, according to reference [1], the presence of lithium (Li) in aluminum (Al) alloys simultaneously increases the elastic limit and decreases density because every 1% Li the density is reduced by about 3% and the elastic limit increased by 6% thus, the Al-Cu-Li alloy 2050-T84 get up as a substitution attractive aluminum-magnesium-zinc alloy 7050-T7451.

The improvement of aeronautical alloys induces the industry to produce materials with lower density and high strength, in this way the aluminum-copper-lithium alloys. The first generation, designated as 2020, was produced in the United States in the 1950s. The manufacture of these alloys was abandoned due to low ductility and poor fracture toughness. The second generation, composed of 2090, 2091 and 8090 alloys, was created as a proposal to improve the resistance to corrosion and its mechanical properties, however, it resulted in alloys with excessive anisotropy and low resistance to stress corrosion cracking. Recently, alloys of the third generation, composed of 2094, 2097, 2099, 2196, AA2197 and 2050 alloys, have been developed for military and aerospace applications and when compared Al-Li alloys of previous generations present high resistance to static and tolerance to damage [2].

The resistance of corrosion of 2xxx series alloys is dependent on their chemical composition and the effect of their elements on the oxide layer. For practical applications, the presence of alloying elements such as Cu, Mg, Mn, Zn, Li, and Si have the purpose of increasing mechanical strength or specific resistance, however these elements form intermetallic particles or precipitated, which are harmful to the corrosion properties of the material, due to the formation of a thinner and more conductive oxide layer that allows the occurrence of cathodic reactions. Avoiding the appearance of these precipitates would be the most effective measure of preventing corrosion, however, the precipitates are important to increase the mechanical properties of the material [3].

These alloys are fabricated by two processes: heat treatments and mechanical forming. Heat treatments perform considerable influence on the corrosive behavior of aluminum alloys as they may result in localized chemical effects and become the material resistant to localized corrosion. When there is no complete solubilization of the alloying elements, the result is a non-uniform microstructure that favors susceptibility to corrosion. The mechanical forming influences the grain morphology and the distribution of the constituent particles of the alloy. The deformation of the material can generate failures in atomic ordering and weaken the oxide layer, allowing localized corrosion [4].

The common forms of corrosion in aluminum alloys are by pits and intergranular, the latter coming from the process of stress corrosion cracking (SCC) and occurs in the contours of grains resulting in poor mechanical properties and brittle fracture of the component when still subject to mechanical requests. The pitting corrosion occurs in isolated points on the metal surface and growth to the inside, often through the material [5].

There are several researches about the behavior of the Al-Cu-Li 2050-T84 alloy, and the microstructural characteristics are presented using the transmission electron microscopy (TEM) technique that showed the presence of precipitates influencing the increase of the strength mechanical of the alloy, fracture toughness,

fatigue and corrosion fatigue at room temperature (23°C), cryogenic (−60°C) and saline environment [6]. The corrosion evaluation was carried out with the potentiodynamic polarization tests and indicated that the alloy in question has a higher value of corrosion potential and pit, when compared to another Al-Li alloys, favoring the formation and growing of pits become pointed enough to results in stress concentration and a crack nucleation contributing directly to the fatigue life of aluminum alloys used in aircraft structures and can result in accelerated failure. However, the results obtained in air, salt spray at 3.5 and 5% NaCl and aqueous saline solution with 3.5% NaCl showed a clear difference in the region of the threshold, however, for the region of Paris independently of the environment, the FCG rates are quite similar.

### 1.1 Microstructural features of 2050-T84 alloy

Aluminum alloys (Al) of the 2xxx series have Copper (Cu) and Lithium (Li) as the main alloying elements and require heat treatments of solubilization, precipitation and aging to improve your mechanical properties. Specifically, the Al-Cu-Li 2050 ternary alloy has density of 2.71 g/cm<sup>3</sup> [7] and presents precipitates responsible for the increase of mechanical strength as  $S'(Al_2CuMg)$ ,  $T_1(Al_2CuLi)$ , and formation of small particles of  $MnAl_6$ ,  $Al_{20}Cu_2Mn_3$ ,  $Al_{12}Mg_2Cr$ , presented by reference [8] through the technique of scanning electron microscopy (SEM) as shown in **Figure 1**. The authors evidenced the formation of precipitates rich in Mg, Zn, Cu and Mn in the grain boundary, which promote reducing of mechanical properties and fracture toughness.

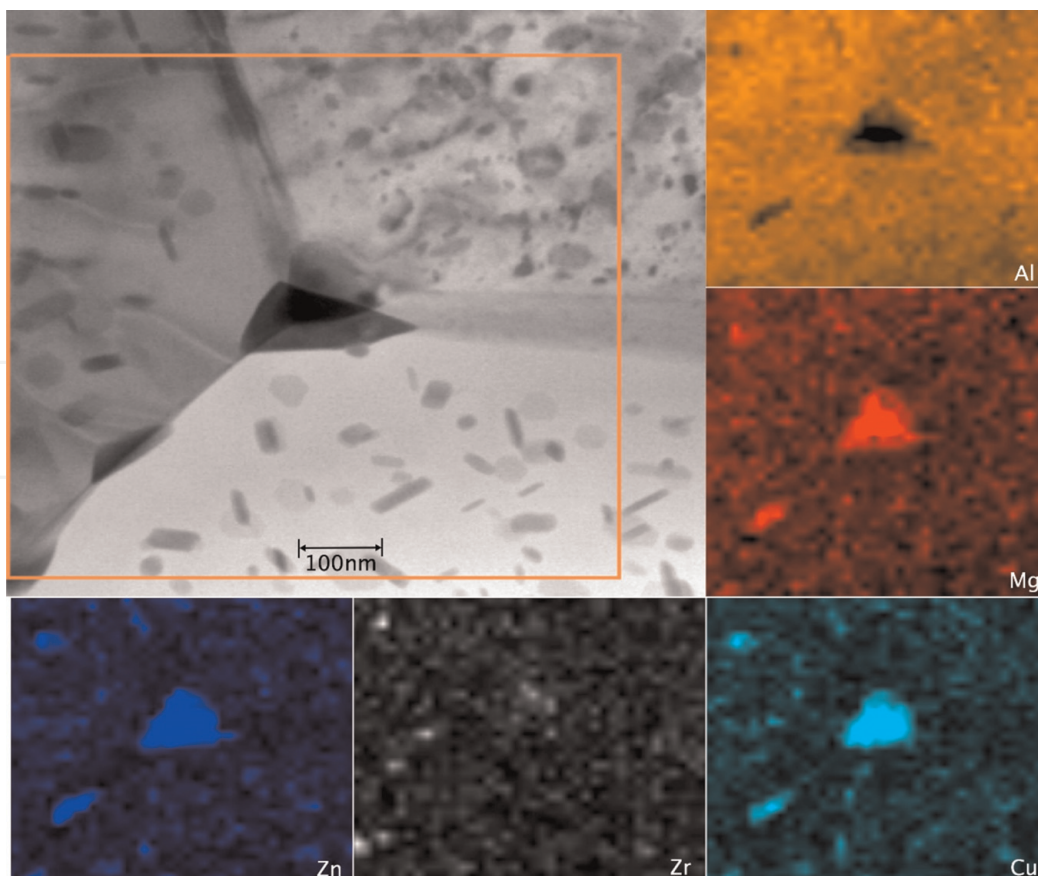


**Figure 1.** Bright field STEM micrograph and respective (EDS) elemental mapping of Al-K, Mn-K, Mg-K, Cu-K and Zn-K in 2050-T84 alloy, showing the composition of precipitates at the grain boundaries (larger) and inside the grain (smaller) on a nanometric scale; bright field TEM micrograph [8].

The presence of  $S'$  in the metal matrix restrains the movements of dislocations and promotes a homogeneous deformation and increases the strength of the alloy. According to Deng et al. [9], the presence of lithium (Li) favors the formation of free zones precipitate (FZP) in the grain boundary, **Figure 2**, which affects fracture properties, increasing the ductility of the material.

Evaluating from corrosion, these properties are not suitable as other aluminum alloys, because under certain conditions they may favor intergranular corrosion and resulting of the embrittlement the material [10].

## 1.2 Effects of corrosion on alloy 2050-T84

By exposing aluminum alloys to the presence of alkaline factors or acidic factors such as chemical ions composed of chlorides or fluorides, e.g., their alumina oxide layer ( $Al_2O_3$ ) can be broken and its degradation accelerated. In 2xxx series alloys, the presence of precipitates containing Cu creates a potential difference between the precipitate and the aluminum matrix resulting in a galvanic cell that makes these materials highly susceptible to corrosion, so that second phase precipitates as  $CuAl_2$  can influence the intergranular corrosion.

Presence of precipitates such as  $Al_6(Cu, Fe, Mn)$  and  $T_1$  in the 2050-T84 alloy may cause pitting corrosion which are cavities that have the bottom in an angular shape and depth generally greater than its diameter. This phenomenon affects corrosion rates, the structural integrity of the component and it is processed in points or in small areas located in the metallic surface in three stages [3]:

- i. Nucleation: is tiny, rapid and leads to the formation of metastable pits due to adsorption of the aggressive ions on the metal surface followed by the rupture of the alumina oxide layer in the most susceptible regions;
- ii. Meta-stable formation: the growth is not fully established, however, is determined by the exposure of the free surface of the metal and by the geometry of the boundary defined during the breakage of the film passive oxide;

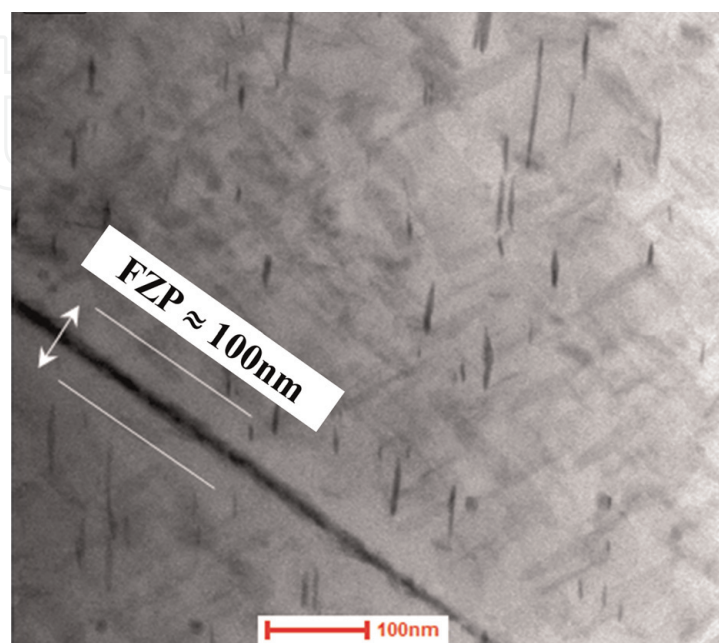


**Figure 2.**

*Imagem de MET evidenciando a zona livre de precipitados da liga de alumio-lítio 2050-T84 [8].*

- iii. Stabilization: occurs after the formation of corrosion products at the entrance of the pits that holds the ions and after several days of exposure, they stop growing and are again passivated. However, if exposed to the medium again the growth of new pitting nucleation sites.

**Figure 3** shows images obtained by SEM reveal the presence of pitting corrosion sites in 2050-T84 alloy when exposed to saline solution. This corrosion process occurred near precipitates and salt crystals deposited on the surface of a sample analyzed by the potentiodynamic polarization tests.

With corrosion evaluation criteria, the addition of lithium is very harmful because this element is highly reactive and additions of about 3% in aluminum causes changes in pitting potential ( $E_{\text{pit}}$ ) leaving the material more vulnerable when exposed to corrosive conditions [3]. With a short time of exposure to the corrosive environment some alloys already have a large number of pits, varying according to the alloy and the environment to which inserted.

This corrosive behavior can be investigated by Evans diagram, obtained through potentiodynamic polarization tests, which provides values for potential corrosion ( $E_{\text{corr}}$ ), pitting potential ( $E_{\text{pit}}$ ) and corrosion current density ( $j_{\text{corr}}$ ) [11]. The corrosion potential is that the anode current process equals the cathode current process. If the anode overvoltage curve is characteristic of a passive metal, at a given potential the pitting nucleation occurs with a sudden surge of current, then the intersection with the cathode overvoltage curve will occur exactly at this potential [12].

### 1.3 Corrosion fatigue in aluminum-copper-lithium alloy 2050-T84

Corrosion fatigue is the term used to denote the damage and failure of components subjected to cyclic loading in a brittle environmental resulting from the interaction between plastic deformation and localized chemical or electrochemical reactions [3–5]. Aluminum alloys have relatively low corrosion resistance if exposed to NaCl salt spray due to the presence of precipitates from heat treatments, which have less corrosion resistance than the matrix. When there is remaking of these precipitates in the grain boundaries there is an increase in susceptibility to intergranular corrosion. Avoiding the emergence of these precipitates would be the

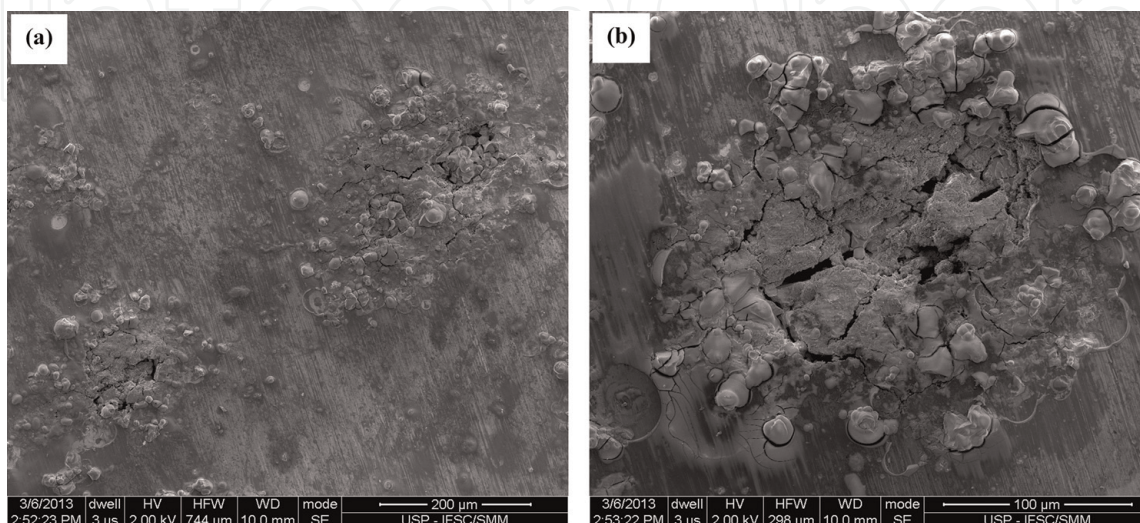


**Figure 3.**  
*Images of 2050-T84 surface alloy by scanning electron microscopy after the potentiodynamic polarization tests. In (a) shows pits and salt crystals in corrosion process, in (b) detail of pit.*

most effective measure of preventing corrosion, however, they are important in enhancing the monotonic mechanical properties of the material [3]. For the reduction of damage caused by the environment, materials less susceptible to corrosion of the environment or the application of surface protection processes such as paints and galvanizing should be used.

In addition to the development complexity of the corrosion fatigue testing methodology, the fatigue crack growth presents adverse behavior in some moments. The crack increases rapidly and in others, cases remain at the same length for hours or even days [3–13]. Interpretation for the fast growth crack, due to the embrittlement of metal alloys subjected to corrosion fatigue, is based on the mechanism of hydrogen embrittlement. Such mechanisms occur due to the reduction of hydrogen particles and the adsorption of atoms at critical locations such as pits, voids between the crack walls and towards the crack tip. Hydrogen atoms, even at room temperature, may be interstitially lodged in the metal crystal or even in grain boundaries, resulting in drastically reducing the toughness and ductility of the material [13].

According to the reference [14] hydrogen induces the appearance of delayed fractures as a consequence of the appearance of numerous surface cracks, which are nucleated throughout the process of leaving hydrogen in the gaseous form of the material. Thus, the FCG rate is accelerated due to the action of hydrogen embrittlement and the presence of oxides that alter the crack closure mechanism.

The plastic deformation at the crack tip causes the oxide layer to break down by exposing the free surface to the corrosive environments and allows for pit. The interior of the pit is more anodic than the rest of the material and in this way the corrosion proceeds to the interior making the pit pointed enough to produce intense

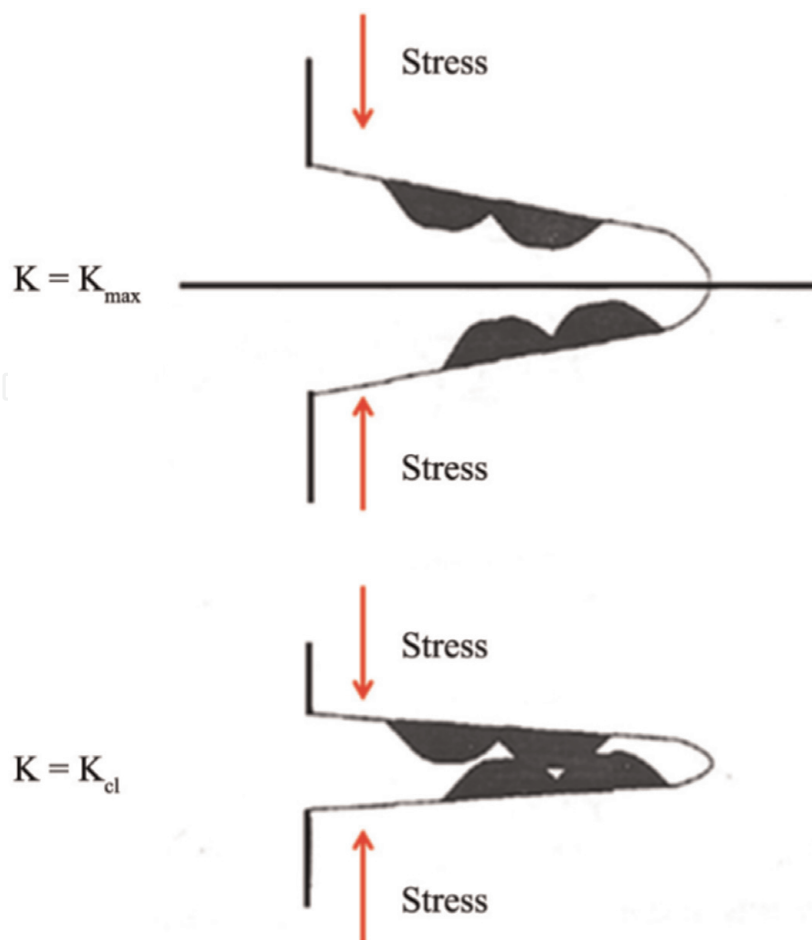


**Figure 4.** Schematic illustration of the wedging effect mechanism induced by corrosion products [6].

concentration of tension and to initiate a crack. If the layer of the repassivation reaction does not occur, the propagation of the crack is continuous [15].

Adversely, there is a possibility that some oxide residue caused by corrosion or salt crystals deposited in front of the crack will deform plasticize the crack tip [16] and with the decrease of the cyclic load the crack tip will not move, it is very thin and closed with a very small radius, as shown in **Figure 4**, and with increased static loading the crack opens elastically and becomes blunting. Under these conditions if the stress at the crack tip is less than or equal to the fracture stress, the crack will not propagate. The final result of the crack propagation rate is due to competition among all of these factors discussed [6].

During the fatigue corrosion tests, the crack growth is controlled by the maximum stress intensity factor  $K_{max}$  and the load ratio (R). Since the corrosive action is a time-dependent phenomenon, corrosion is most evident at low frequencies due to the greater integration between the environment and the material, increasing the embrittlement of the crack. Jones et al. [17], investigated the effect of corrosion on crack nucleation of the 2024-T3 alloy at various levels of fatigue crack growth and identified nucleation from pits that emerged during the corrosion process and concluded that the aggressive condition accelerates nucleation and crack growth in regions close to the threshold.

The action of chemical elements at the crack tip was studied by Wang [16] in corrosion fatigue tests with 3.5% NaCl in aluminum alloys. The authors verified there was a variation of the stress intensity factor at the threshold and increase in the fatigue crack growth rate ( $da/dN$ ) and also concluded that the ratio between stresses has an influence in the region close to the threshold and as the ratio increases, the variation of the factor of intensity decreases.

## 2. Methods and materials

The material of this study is an aluminum-lithium alloy 2050 with the T84 heat treatment indicates that it was obtained through the solubilization steps with the temperature between 480 and 540°C, cold rolling, stress relief and natural aging hardening as shown in Ref. [7] and the chemical composition described in **Table 1**.

This material it was provided as plate with 800 × 550 × 50 mm from which they were extracted specimens for potentiodynamic polarization, tensile, toughness, fatigue and corrosion fatigue tests. Potentiodynamic polarization performed in triplicate followed the ASTM G61 [18] standard and the measurements were made in the range -1.2 to -0.2 V with a potential sweep rate of 0.5 mV s<sup>-1</sup> using a GAMRY reference 600 potentiostat/galvanostat, with 3.5% NaCl, aerated at 23°C resulted in the values of  $E_{corr}$  and  $j_{corr}$  obtained by the curve.

Tensile tests were carried out according to the ASTM E8/E8M [19] standard, using 05 specimens removed longitudinally to the sheet rolling direction, see **Figure 5**. The fracture toughness were carried out according to the ASTM E399 [20] standard in in MTS servo-hydraulic testing machine, with the clip gage to measure the crack size using the compliance technique and specimens with C(T)

Li	Cu	Mg	Mn	Zr	Ag	Si	Ti	Cr	Fe	Ni	Zn	Al
0.87	3.54	0.31	0.37	0.08	0.37	0.03	0.03	0.06	30*	0.02	<1*	Base

\*ppm – part per million

**Table 1.**  
 Nominal chemical composition of aluminum-lithium alloy 2050-T84 (wt%) [7].



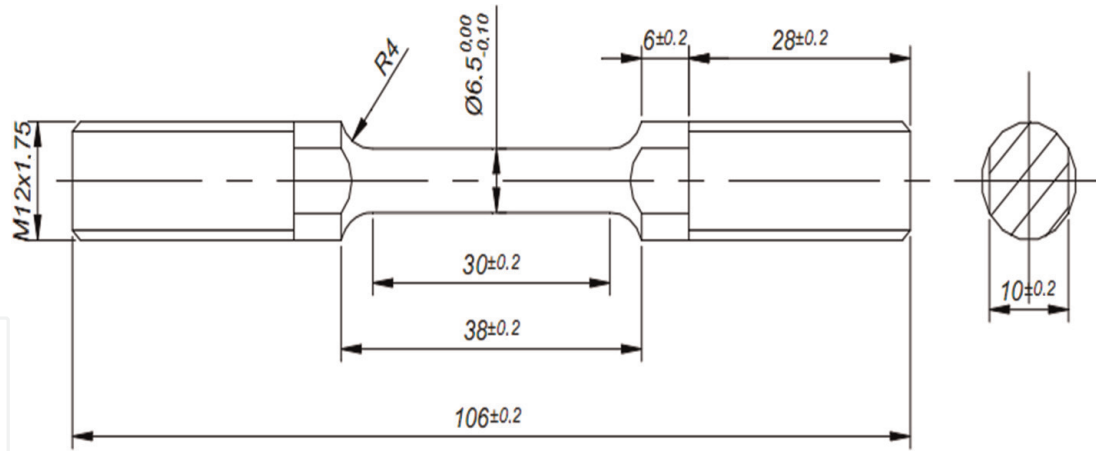


**Figure 5.**  
Dimensions in millimeter of specimens to tensile test at room and cryogenics temperatures.

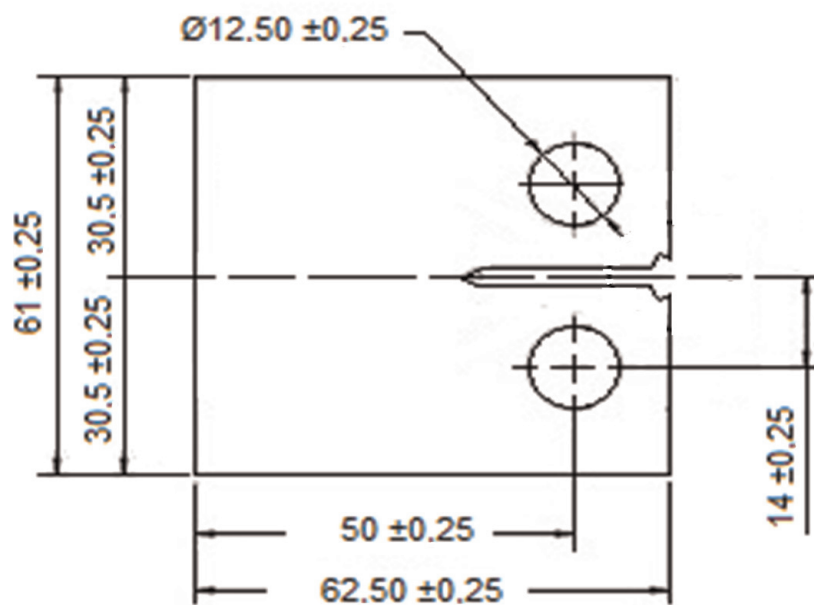


**Figure 6.**  
Geometry and dimensions of specimens to fracture toughness tests at room and cryogenics temperatures (thickness (B) 25.4 mm)).

geometry removed at direction TL and LT, thickness (B) 25.4 mm and geometry and dimensions shown in **Figure 6**. Both tests were conducted at 23 and  $-60^{\circ}\text{C}$  at a chamber with liquid nitrogen.

Fatigue crack growth and corrosion fatigue were performed in air with a frequency of 15 Hz, 3.5 and 5% NaCl salt spray and with 3.5% NaCl aqueous saline solution. Specimens with C(T) geometry and extracts in the LT direction according to the specifications of ASTM E399 [20], thickness (B) 12.5 mm were tested in a MTS servo-hydraulic machine, according to the specifications of ASTM E647 [21], with sinusoidal waveform, extensometry and load ratio  $R(K_{\min}/K_{\max})$ , Poisson's coefficient if  $\nu = 0.33$  and intensity gradient  $C = -0.787$ . From the region II of curves, the coefficient ( $m$ ) of the linear regression line of the equation proposed by de Paris and Edorgan (Eq. (1)) was determined and the coefficient found by the extension of the straight line.

$$\frac{da}{dN} = C(\Delta K)^m, \quad (1)$$

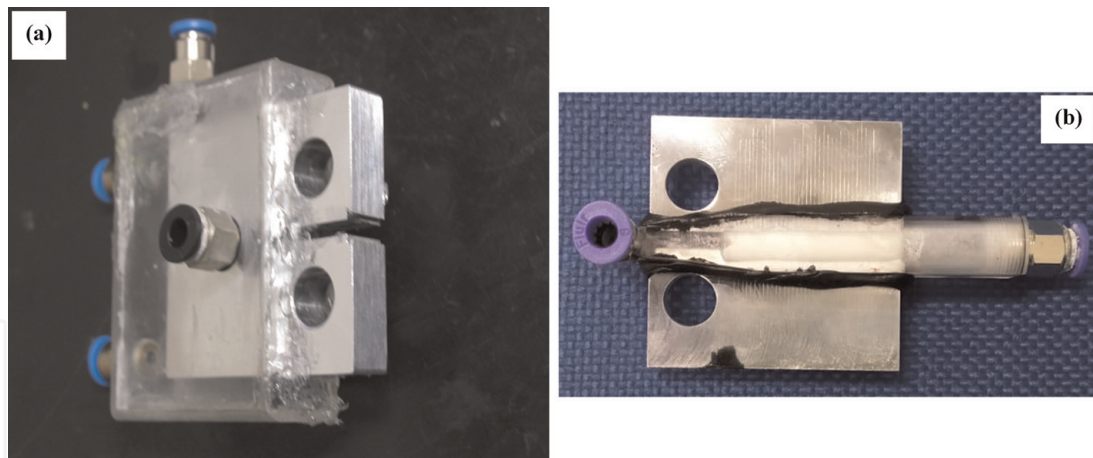


**Figure 7.** Fatigue crack growth specimens mounted for testing. In (a) for tests in salt spray with 3.5 and 5% NaCl (thickness (B) 12.5 mm). In (b) for tests in aqueous solution with 3.5% NaCl (thickness (B) 6 mm).

Where  $da/dN$ : fatigue crack growth rates, C: constant,  $\Delta K$ : variation of the stress intensity factor,  $m$ : coefficient of the linear regression line of the equation proposed by de Paris and Edorgan.

The corrosion fatigue tests in 3.5 and 5% salt spray were conducted with C(T) specimens, see **Figure 6**, mounted inside fog cell coupled to a salt spray generation and conditioning device consisting of an air compressor, a reservoir of saline solution and nebulizer. **Figure 7(a)** shows the test specimen whose flow rate was 0.084 ml/s. The threshold values for air and salt spray tests were estimated from a linear regression of the fatigue crack growth rate curve as a function of the variation of the stress intensity factor ( $da/dN \times \Delta K$ ), using at least 5 points between  $10^{-6}$  and  $10^{-7}$  mm/ciclo rates of and therefore, this procedure was adopted. A curve in the propagation stage II was obtained for the tests in aqueous saline solution, conducted with 1 Hz and a flow rate of 14.70 ml/s. The fog cell was positioned in such a way that integrity and the free circulation of saline solution were guaranteed by the inlet and outlet of the system as shown in **Figure 7(b)**.

### 3. Results

#### 3.1 Potentiodynamic polarization

Results of potentiodynamic polarization shown in **Figure 8(a)** and from the curve shown in **Figure 8(b)** the  $E_{pit}$ . These results were listed and compared with the Al-Cu-Li-Mg 2198-T851 alloy as shown in **Table 2**.

Evaluating the results of  $E_{corr}$ , close values between both alloys, however, the  $j_{corr}$  of the 2050-T84 alloy is larger indicating that this material has a higher dissolution rate. As seen in **Figure 8(b)**,  $E_{pit}$  has been determined when the current value increases abruptly due to breakage of the insulating and passivating film, changing the orientation of the curve. When comparing two alloys, ensure that the 2050-T84 alloy has a slightly more negative volt than the 2198-T851 alloy, indicating that the alloy requires more energy yielded to begin the corrosion process and that although the alloy 2050-T84 require less amount of energy yielded, once the process is started the material is corroded with higher speed.

Presence of precipitates  $T_1$  and  $T_2$  and results in an inversion of the corrosion mechanism. First, these precipitates are anodic, resulting in the dissolution thereof however, during the corrosion process, the Li is preferably dissolved, resulting in an

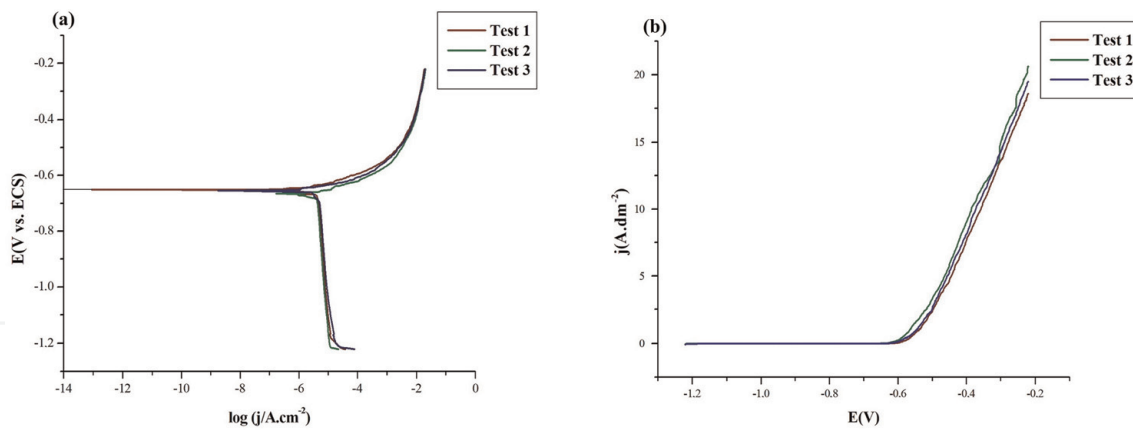


**Figure 8.** Potentiodynamic polarization plots obtained for aluminum-lithium in (a) corrosion potential; in (b) pitting potential.

Alloy	E (V)	Log J	E (pit)
2050-T84	-0.6581	-3.963	-0.601
2198-T851	-0.667	-2.711	-0.587

**Table 2.** Results obtained of potentiodynamic polarization for aluminum-lithium alloys 2198 T851 and 2050 T84.

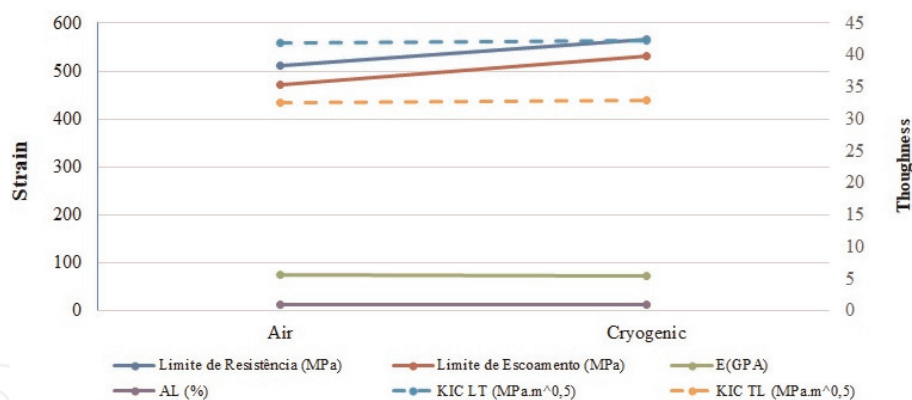


**Figure 9.** Tensile and toughness properties of alloy 2050-T84.

increase in the amount of Cu on the surface. Consequently, the corrosion potential increases to more positive values, causing matrix dissolution [6].

### 3.2 Mechanical behavior and toughness of 2050-T84 alloy

Evaluation of the mechanical and tenacity behavior of high strength aluminum alloys is performed according to the types of stresses requested and operating temperature because they are materials used in structures of vehicles, pipelines, pressure vessels, aircraft fuselage and reservoir of storage hydrogen and oxygen liquids that are mechanically requested at ambient and/or cryogenic temperatures as described by reference [11]. Such applications are possible because of their low

density, high specific strength, non-magnetism, stable microstructure, high elastic limit, and ductility retention.

Mechanical behavior and fracture toughness of the 2050-T84 alloy at the air at 23°C and cryogenic at -60°C are shown in **Figure 9**. Results showed no significant difference with temperature variation and can be attributed to the retention of ductility at cryogenic temperatures due to the face-centered cubic crystal structure (FCC) and the and the freezing of impurities with low melting point and rich in hydrogen (H), sodium (Na) and potassium (K), dispersed in the Al matrix [15].

Influence of temperature on fracture toughness  $K_{IC}$  was evaluated with specimens for analysis machined in TL and LT orientation. The values of the LT orientation are higher and reveal anisotropy of the material related to the characteristics of the recrystallized grains. Another important point that explains this concept is the crystallographic and morphological texture produced by the rolling, associated with the FZP and the distribution of the constituent particles in the material. These factors determine a preferred sense for the of intergranular crack growing and intrinsic plastic anisotropy of the material [16]. Additionally, when the stresses at the crack tip are high, the resistance to deformation is lower and provides the intergranular fracture. With lower ductility and high loading, the crack growing rapidly and the fracture toughness of the material decreases.

### 3.3 Fatigue crack growth and corrosion-fatigue

The plots are shown in **Figure 10** and was determined the coefficient found by the extension of the straight line as shown **Table 3**. Evaluating the threshold ( $\Delta K_0$ ) results for tests conducted in air and 3.5 and 5% salt spray where can be verified in the tests conducted in salt spray, the corrosive action is the most influential variable

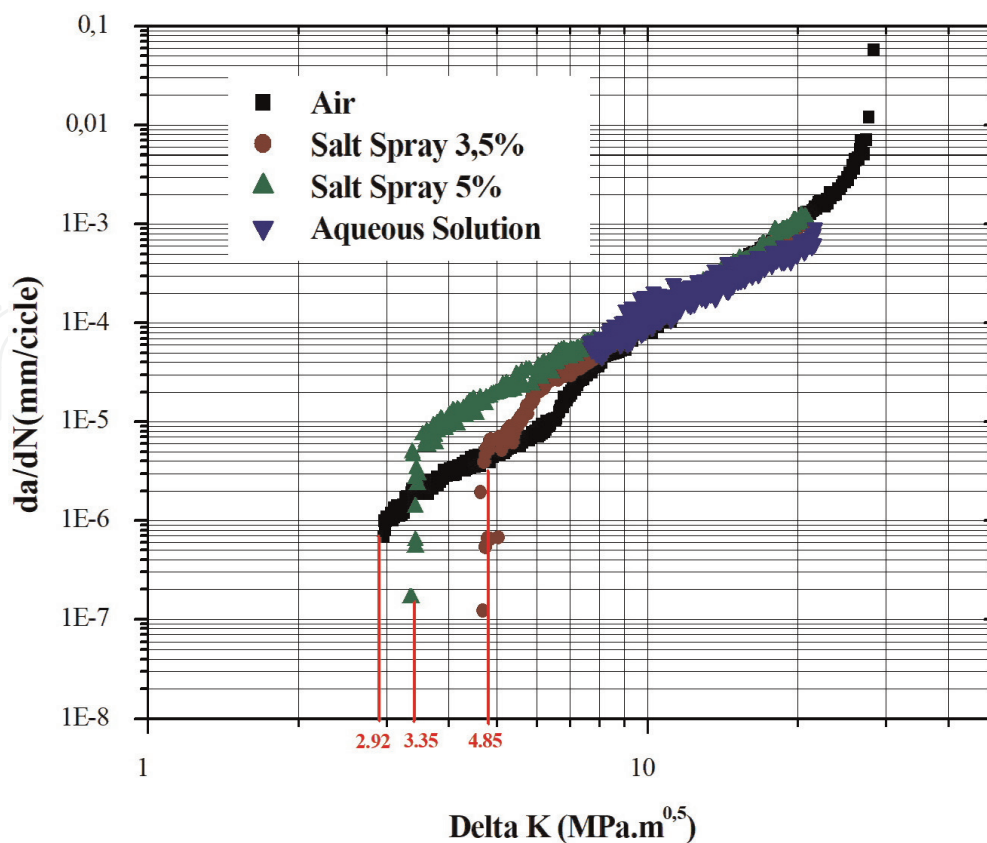


**Figure 10.**  $da/dN \times \Delta K$  curves for the 2050-T84 in air, salt spray at 3.5 and 5% of NaCl and aqueous solution with  $R = 0.1$ .

Condition	Paris	R <sup>2</sup>	$\Delta K_0 (MPa\sqrt{m})$
Air	$da/dN = 5.04E - 08(\Delta K)^{2.89}$	0.99	2.92
Salt spray 3.5%	$da/dN = 2.14E - 08(\Delta K)^{2.97}$	0.99	4.85
Salt spray 5%	$da/dN = 3.22E - 08(\Delta K)^{3.02}$	0.99	3.35
Aqueous solution	$da/dN = 7.19E - 08(\Delta K)^{2.41}$	0.97	—

**Table 3.**

Aluminum-lithium's constant  $C$  and  $m$  for the Paris-Erdogan equation and threshold.

due to the action of the environment the loading action overlaps and may increase or reduce the crack growth rate and the propagation rate. Observed that there is an acceleration of the propagation rate and as this value increases, the behavior in salt spray is similar to that of the behavior in air with a slight influence on the FCG of the test carried out in aqueous saline solution that presents a tendency to increase the critical stress intensity factor indicating improvement of the fracture toughness to the increase of the plastic zone at the crack tip.

Lowest threshold value was found with the test conducted in air. This is due to the common factors influencing the crack closure, such as the induction of plasticity, the formation of oxides in front of the crack and/or the roughness generated on the fracture surface, due to the severity of the loading. The curve obtained with a salt spray of 3.5% NaCl presented a higher threshold indicating a significant influence of the action of the oxides residues or salt crystals deposited on the surface of the crack that possibly induced the plastic deformation and avoided the embrittlement action of the fog. Considering that the 5% NaCl test curve accelerates discretely from the region close to the threshold, is possible that hydrogen embrittlement and anodic dissolution acted preferentially in the crack growth process, forming surface oxides and increasing the fatigue crack growth rate in the Paris region by reducing the threshold values.

In these conditions the fracture micromechanism occurred due to the movement of the slip bands that favored the rupture of the oxide layer and the surface of the metal was exposed to the saline solution making it anodic, whereas the regions adjacent to the sliding became cathodic forming an electrochemistry heaped load that, together with hydrogen embrittlement, accelerated crack growth and resulted in a lower threshold. Although no threshold result was obtained with tests conducted in aqueous saline solution, the final result of the crack propagation rate in this region is due to the competition between hydrogen embrittlement and the plasticity induced by crystals of salt and oxides, therefore it is a very complex micromechanism.

According to Wang [16], when the corrosion occurs simultaneously with fatigue loading, is expected to result in reduced material properties due to slip bands on the material, grain handling, free surface corrosion at the crack tip and crack closure, however, this did not occur with the 2050-T84 alloy. These results show that there is a clear difference of the threshold region when the tests were conducted in salt spray, however, for the Paris region regardless of the environment, the rates of FCG are quite similar. For Moreto et al. [6] this behavior occurs for two reasons, the first is related to the process of crack growth being purely mechanical because, a short time of interaction with the environment and the second reason is based on the concepts of crack closure, which when fully opened, the corrosion products formed within the crack lead to contact between the surfaces by raising the crack closing tension intensity factor.

## 4. Discussion

The 2050-T84 alloy with additional lithium was developed to have improved mechanical properties to be applied to aircraft structural components. The results of potentiodynamic potential shows that this alloy requires less amount of energy yielded for rupture of the oxide layer, however, once corrosion is started its evolution is rapid. Corrosion process occurred near precipitates  $T_1$  and  $T_2$  that increases to more positive values, causing matrix dissolution. However, the presence of the lithium to weight reduction and increase of mechanical resistance due to the appearance of precipitate  $T_1$  and free zones precipitate. In cryogenic conditions, this material presents retention of ductility and fracture toughness, due to the face-centered cubic crystal structure (FCC) and the and the freezing of impurities with low melting point and rich in hydrogen (H), sodium (Na) and potassium (K), dispersed in the Al matrix.

Fatigue corrosion behavior of this material indicates that the competition between hydrogen embrittlement and the plasticity induced by salt crystals and cracking tip oxides are beneficial for FCG. This behavior occurs for to process of crack growth being purely mechanical and the corrosion products formed within the crack lead to contact between the surfaces by raising the crack closing tension intensity factor.

## Acknowledgements

The authors would like to thanks CAPES for the financial support, EMBRAER supply the material and the Department of Materials, São Carlos School of Engineering, University of São Paulo for the use of the experimental facilities.

## Author details

Maciel Carla Isabel dos Santos<sup>1\*</sup>, Bose Filho Waldek Wladimir<sup>2</sup>  
and Ruchert Cassius Olívio Figueiredo Terra<sup>3</sup>


1 Paulista State University “Júlio de Mesquita Filho”, Bauru, SP, Brazil

2 São Carlos Engineering School, University of Sao Paulo, São Carlos, SP, Brazil

3 Lorena Engineering School, University of Sao Paulo, Lorena, SP, Brazil

\*Address all correspondence to: [carla.ism@usp.br](mailto:carla.ism@usp.br)

## IntechOpen

© 2019 The Author(s). Licensee IntechOpen. This chapter is distributed under the terms of the Creative Commons Attribution License (<http://creativecommons.org/licenses/by/3.0>), which permits unrestricted use, distribution, and reproduction in any medium, provided the original work is properly cited. 

## References

- [1] Fendoni A. The effect of post weld heat treatment on the corrosion behaviour of a Aa2050T34-Fsw [thesis]. Birmingham: University of Birmingham; 2009
- [2] Starke EA. Historical Development and Present Status of Aluminum-Lithium Alloys. Amsterdam: Elsevier Inc.; 2013
- [3] Ghali E. Corrosion Resistance of Aluminum and Magnesium Alloys: Understanding, Performance, and Testing. Hoboken: John Wiley & Sons; 2010
- [4] Jagan Reddy G, Wanhill RJH, Gokhale AA. Mechanical Working of Aluminum-Lithium Alloys. Amsterdam: Elsevier Inc.; 2013
- [5] Piascik RS, Gangloff RP. Environmental fatigue of an Al-Li-Cu alloy: Part I. Intrinsic crack propagation kinetics in hydrogenous environments. *Metallurgical Transactions A*. 1991; **22**(10):2415-2428
- [6] Moreto JA et al. Environmentally-assisted fatigue crack growth in AA7050-T73511 al alloy and AA2050-T84 Al-Cu-Li alloy. *Materials Research*. 2015; **18**(6):1291-1297
- [7] Aerospace Material Specification. SAE AMS 4413—Aluminum alloy plate—3.5Cu-1.0Li-.40Mg-.35Mn-.012Zr (2050-T84) . West Conshohocken: SAE Aerospace International Group; 2007. pp. 1-5
- [8] Chemin AEA, Afonso CM, Pascoal FA, Maciel CI dos S, Ruchert COFT, et al. Characterization of phases, tensile properties, and fracture toughness in aircraft-grade aluminum alloys. *Material Design & Processing Communications*. 2019; **1**(4):1-13
- [9] Deng YL, Yang JL, Li SY, Zhang J, Zhang XM. Influence of Li addition on mechanical property and aging precipitation behavior of Al-3.5Cu-1.5Mg alloy. *Transactions of Nonferrous Metals Society of China (English Edition)*. 2014; **24**(6):1653-1658
- [10] ASM International. Handbook Committee. Properties and Selection: Nonferrous Alloys and Special-Purpose Materials. Vol. 2. Ohio: ASM International; 2001
- [11] Hafley RA, Domack MS, Hales SJ, Shenoy RN. Evaluation of Aluminum Alloy 2050-T84 Microstructure and Mechanical Properties as Ambient and Cryogenic Temperatures. Hampton, Virginia: National Aeronautics and Space Administration. Nasa Center for Aerospace Information; 2011. p. 81
- [12] Anderson TL. Fracture Mechanics Fundamentals and Applications. 3rd ed. New York: Taylor & Francis Group; 2005
- [13] Perng TP, Altstetter CJ. Hydrogen effects in austenitic stainless steels. *Materials Science and Engineering A*. 1990; **129**(1):99-107
- [14] Samui AB, Patankar AS, Rangarajan J, Deb PC. Study of polyaniline containing paint for corrosion prevention. *Progress in Organic Coatings*. 2003; **47**(1):1-7
- [15] Moreto JA, Gamboni OC, Marino CEB, Bose Filho W, Fernandes JCS, Rocha LA. Corrosion behavior of Al and Al-Li alloys used as aircraft materials. *Corrosion and Protection of Materials*. 2012; **31**(34):60-64
- [16] Wang R. A fracture model of corrosion fatigue crack propagation of aluminum alloys based on the material elements fracture ahead of a crack tip. *International Journal of Fatigue*. 2008; **30**(8):1376-1386

[17] Jones K, Shinde SR, Clark PN, Hoepfner DW. Effect of prior corrosion on short crack behavior in 2024-T3 aluminum alloy. *Corrosion Science*. 2008;**50**(9):2588-2595

[18] ASTM. ASTM G61-Standard Test Method for Conducting Cyclic Potentiodynamic Polarization Measurements for Localized Corrosion Susceptibility of Iron, Nickel or Cobalt Based Alloys. West Conshohocken: ASTM International; 2010

[19] ASTM Standard. E8/E8M—16a Standard Test Methods for Tension Testing of Metallic Materials. West Conshohocken: ASTM International; 2016

[20] ASTM E399-12. Standard Test Method for Linear-Elastic Plane-Strain Fracture Toughness  $K_{Ic}$  of Metallic Materials. West Conshohocken: ASTM International; 2013

[21] ASTM International. ASTM E647—Standard Test Method for Measurement of Fatigue Crack Growth Rates. Finland: University of Oulu; 2015. pp. 1-49

IntechOpen